Enhanced Modern Heat Transfer to the Arctic by Warm Atlantic Water

Robert F. Spielhagen, *et al.*

Science **331**, 450 (2011);
DOI: 10.1126/science.1197397

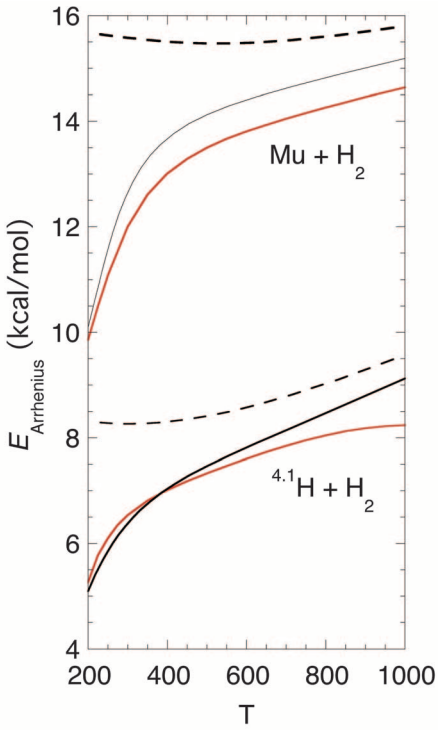

Fig. 4. Comparison of Arrhenius activation energies ($E_a \equiv E_{Arrhenius}$) calculated via QM (red solid lines), ICVT (dashed black lines), and ICVT/LAG (solid black lines) for the reactions of $^{4.1}$H and $^{0.11}$H with H_2 as a function of temperature (T).

(within 23%) of the VTST calculations with experiment lends credence to the existence of quantized transition states (*26*, *27*) with these large amounts of vibrational energy.

The tunneling transmission coefficient, which is the ratio of the ICVT/LAG rate constant to the ICVT rate constant, is 4.3, 2.1, and 1.6 at 295, 405, and 500 K, respectively. Reactions of $^{0.11}$H may exhibit greater tunneling effects than heavier isotopes because of the small mass (*6*), and this would be true in any one-dimensional treatment with an isotope-independent effective barrier. However, the LAG approximation is multidimensional, including ZPE effects (*28*, *29*) in the effective tunneling barriers and isotope-dependent tunneling paths, and the effective barrier to tunneling is much broader for the $^{0.11}$H case because of the large ZPE of the $^{0.11}$H^{1}H product (*30*). It is very encouraging that the results based on the LAG tunneling treatment, which is affordable for complex systems (*31*), correctly accounts for the KIE despite the quite different effective potentials for the two isotopes, confirming the physicality of the isotope-dependent barriers.

The Arrhenius (*32*) activation energy is defined as

$$E_a = -R\frac{d\ \ln\ k}{d(1/T)} \qquad (1)$$

which is proportional to the negative slope of an Arrhenius plot. It is well known (*33*, *34*) that E_a can exhibit substantial temperature dependence, and the present reactions illustrate this in Fig. 4; this kind of detail cannot be revealed yet by experiment. Figure 4 shows that E_a would be quite different in magnitude and temperature dependence without tunneling, but with tunneling, the ICVT/LAG calculation agrees very well with the dramatic temperature dependence and isotope dependence shown by the accurate quantum-dynamical results. These results confirm the usefulness of VTST for interpreting large quantum effects.

References and Notes

1. A Kohen, H.-H. Limbach, Eds., *Isotope Effects in Chemistry and Biology* (Taylor & Francis, Boca Raton, FL, 2006).
2. M. Born, J. R. Oppenheimer, *Ann. Phys.* **84**, 457 (1927).
3. J. Espinosa-Garcia, *Phys. Chem. Chem. Phys.* **10**, 1277 (2008).
4. D. C. Walker, *J. Phys. Chem.* **85**, 3960 (1981).
5. S. Baer *et al.*, *ACS Symp. Ser.* **502**, 111 (1992).
6. T. Tanaka, T. Takayanagi, *Chem. Phys. Lett.* **496**, 248 (2010).
7. D. J. Arseneau *et al.*, *Physica B* **404**, 946 (2009).
8. G. Audi *et al.*, *Nucl. Phys. A.* **729**, 3 (2003).
9. J. V. Michael, K. P. Lim, *Annu. Rev. Phys. Chem.* **44**, 429 (1993).
10. S. L. Mielke *et al.*, *Phys. Rev. Lett.* **91**, 063201 (2003).
11. I. D. Reid *et al.*, *J. Chem. Phys.* **86**, 5578 (1987).
12. D. G. Truhlar, B. C. Garrett, *Acc. Chem. Res.* **13**, 440 (1980).
13. A. Dybala-Defratyka, P. Paneth, R. Banerjee, D. G. Truhlar, *Proc. Natl. Acad. Sci. U.S.A.* **104**, 10774 (2007).
14. Experimental details, including scheme S1, are in the SOM on *Science* Online.
15. P. A. Souder *et al.*, *Phys. Rev. A* **22**, 33 (1980).
16. M. Senba *et al.*, *Phys. Rev. A* **74**, 042708 (2006).
17. M. Born, K. Huang, *The Dynamical Theory of Crystal Lattices* (Oxford Univ. Press, London, 1954).
18. S. L. Mielke, B. C. Garrett, K. A. Peterson, *J. Chem. Phys.* **116**, 4142 (2002).
19. S. L. Mielke, D. W. Schwenke, G. C. Schatz, B. C. Garrett, K. A. Peterson, *J. Phys. Chem. A* **113**, 4479 (2009).
20. Y. Sun *et al.*, *Phys. Rev. A* **41**, 4857 (1990).
21. B. C. Garrett, D. G. Truhlar, R. S. Grev, A. W. Magnusson, *J. Phys. Chem.* **84**, 1730 (1980).
22. B. C. Garrett, D. G. Truhlar, *J. Phys. Chem.* **79**, 4931 (1983).
23. B. C. Garrett, D. G. Truhlar, *J. Chem. Phys.* **81**, 309 (1984).
24. B. C. Garrett, D. G. Truhlar, *J. Phys. Chem.* **95**, 10374 (1991).
25. C. F. Bernasconi, Ed., *Investigation of Rates and Mechanisms of Reactions* (Wiley, New York, ed. 4, 1986).
26. D. C. Chatfield, R. S. Friedman, D. G. Truhlar, D. W. Schwenke, *Faraday Discuss. Chem. Soc.* **91**, 289 (1991).
27. D. C. Chatfield, R. S. Friedman, D. W. Schwenke, D. G. Truhlar, *J. Phys. Chem.* **96**, 2414 (1992).
28. R. A. Marcus, *J. Chem. Phys.* **41**, 610 (1964).
29. A. Kuppermann, D. G. Truhlar, *J. Am. Chem. Soc.* **93**, 1840 (1971).
30. B. C. Garrett *et al.*, *Hyperfine Interact.* **32**, 779 (1986).
31. R. Meana-Pañeda, D. G. Truhlar, A. Fernández-Ramos, *J. Chem. Theory Comput.* **6**, 6 (2010).
32. S. Arrhenius, *Z. Physikal. Chem* **4**, 226 (1889).
33. N. C. Blais *et al.*, *J. Phys. Chem.* **85**, 1094 (1981).
34. B. C. Garrett *et al.*, *J. Am. Chem. Soc.* **108**, 3515 (1986).

35. We thank the Natural Sciences and Engineering Research Council of Canada, the Office of Basic Energy Sciences of the U.S. Department of Energy (DOE), and the Air Force Office of Scientific Research for their support of this work. Battelle operates the Pacific Northwest National Laboratory for DOE.

Supporting Online Material

www.sciencemag.org/cgi/content/full/331/6016/448/DC1
Methods
Scheme S1
References

22 October 2010; accepted 7 December 2010
10.1126/science.1199421

Enhanced Modern Heat Transfer to the Arctic by Warm Atlantic Water

Robert F. Spielhagen,[1,2]* Kirstin Werner,[2] Steffen Aagaard Sørensen,[3] Katarzyna Zamelczyk,[3] Evguenia Kandiano,[2] Gereon Budeus,[4] Katrine Husum,[3] Thomas M. Marchitto,[5] Morten Hald[3]

The Arctic is responding more rapidly to global warming than most other areas on our planet. Northward-flowing Atlantic Water is the major means of heat advection toward the Arctic and strongly affects the sea ice distribution. Records of its natural variability are critical for the understanding of feedback mechanisms and the future of the Arctic climate system, but continuous historical records reach back only ~150 years. Here, we present a multidecadal-scale record of ocean temperature variations during the past 2000 years, derived from marine sediments off Western Svalbard (79°N). We find that early–21st-century temperatures of Atlantic Water entering the Arctic Ocean are unprecedented over the past 2000 years and are presumably linked to the Arctic amplification of global warming.

Rising air temperatures (*1*–*3*) and a decline of the sea ice cover (*4*, *5*) evidence a rapid warming in the Arctic that has reversed a long-term cooling trend (*6*). Relatively warm Atlantic Water (AW) in the Fram Strait Branch (FSB) of the North Atlantic Current is the major carrier of oceanic heat to the Arctic Ocean (Fig. 1). It maintains perennially ice-free conditions in the eastern Fram Strait today and supplies salt to the intermediate and bottom waters of the Arctic Ocean, thereby stabilizing the stratification (*7*, *8*). In the eastern Fram Strait, AW with temperatures of 2° to 6°C and salinities of >35.0 is found at 50- to 600-m water depth (Fig. 2). Most of the year it is overlain by a mixed layer of lower salinity, seasonally variable temperatures, and ice coverage in ex-

[1]Academy of Sciences, Humanities, and Literature, 53151 Mainz, Germany. [2]Leibniz Institute of Marine Sciences (IFM-GEOMAR), 24148 Kiel, Germany. [3]Department of Geology, University of Tromsø, 9037 Tromsø, Norway. [4]Alfred Wegener Institute of Polar and Marine Research, 27515 Bremerhaven, Germany. [5]Department of Geological Sciences and Institute of Arctic and Alpine Research, University of Colorado, Boulder, CO 80309, USA.

*E-mail: rspielhagen@ifm-geomar.de

treme winters. These parameters also varied in the past 2000 years, as shown by sea ice observations and sediment core studies (*5*, *9*).

Highly variable AW advection to the Arctic in the Late Quaternary has been recorded by proxies like microfossil abundances, flux rates, and species ratios (subpolar versus polar species) in sediment cores. Advection maxima occurred mostly during relatively warm periods (interglacials and interstadials) (*10*–*12*). The Holocene [past 12 ky (ky, thousand years)] was characterized by a thermal maximum at 10 to 9 ky and a cooling thereafter (*13*). Previous studies, however, were unable to clearly resolve variations within a few hundred years or less. Such variations are well known from historical and proxy data of European climate (*14*) and subdivide the last 2 ky into the Roman Warm Period (RWP, until ~600 CE), the Dark Ages Cold Period (DACP, ~600 to ~900 CE), the Medieval Climate Anomaly (MCA, ~900 to ~1500 CE), the Little Ice Age (LIA, ~1500 to ~1900 CE), and the Modern (Industrial) Period. Ages of boundaries between individual periods may vary regionally.

To reconstruct the temperature variability of AW in the FSB within the past ~2000 years, we investigated planktic foraminifers in a sediment core obtained in August 2007 from the western Svalbard continental margin at site MSM5/5-712 (Fig. 1). This site is strategically situated in the path of AW inflow to the Arctic Ocean. Radiocarbon dates in core MSM5/5-712-1 (table S1) revealed sedimentation rates of 18 to 20 cm ky^{-1} for the period 120 BCE to 1475 CE and 27.7 cm ky^{-1} thereafter, resulting in a resolution of 28 and 18 years per 0.5-cm sample, respectively (Fig. 3). The core top had a modern age. Bioturbation by bottom-living organisms is expected to somewhat smooth paleoenvironmental signals, but a quantification of the effect is difficult. Our temperature reconstruction of AW inflow to the Arctic Ocean is based on two independent methods: (i) The SIMMAX modern analog technique (*15*) applied on planktic foraminifer species counts to calculate temperatures at 50-m water depth and (ii) Mg/Ca measurements on the species *Neogloboquadrina pachyderma* (sinistral). Method details are given in the Supporting Online Material (SOM). Habitat and calcification depth of planktic foraminifers in the eastern Fram Strait are below 50-m water depth and reach down to ~300 m, but the distribution maximum is above 150 m (*16*). In this area, plankton blooms usually occur in August (*16*). Thus, our temperature reconstructions reflect mid-summer conditions in the uppermost part of the AW layer, averaged over a few decades.

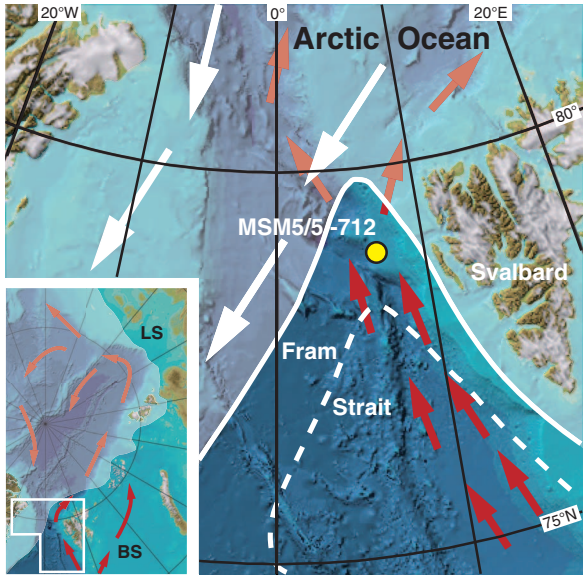

Fig. 1. Bathymetric map of the Fram Strait area and the eastern Arctic Ocean (inset; source: www.ibcao.org). Average sea ice coverage for April [1989 to 1995; stippled line: 1963 to 1969 (*31*)] and September (inset; 1979 to 2000; source: http://nsidc.org) is indicated by white shading. White arrows indicate ice flow direction in Fram Strait area. Red arrows indicate flow direction of Atlantic Water. Atlantic water flow is below halocline waters in the Arctic Ocean proper. Yellow spot marks station MSM5/5-712 at 78°54.94'N, 6°46.04'E, 1491-m water depth. BS, Barents Sea; LS, Laptev Sea.

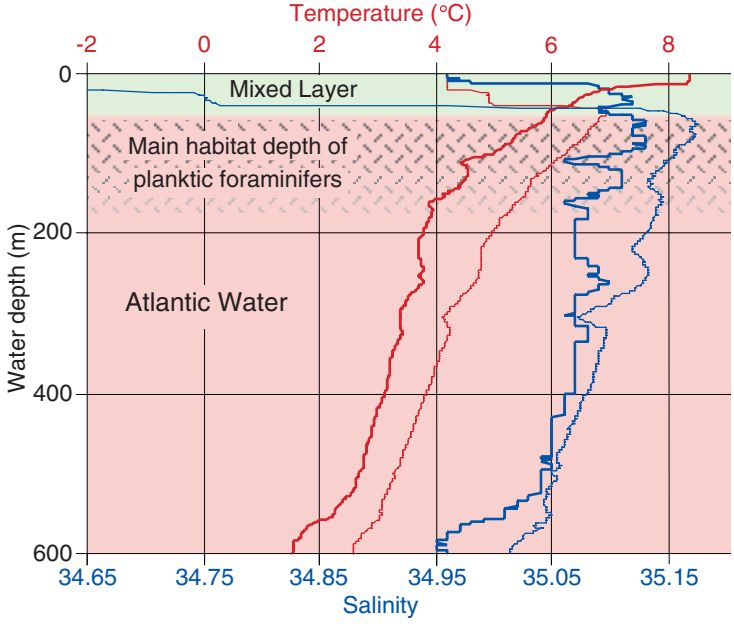

Fig. 2. Water-mass structure of the upper 600 m at station MSM5/5-712. Seasonal variability of temperature (red lines) and salinity (blue lines) in the Atlantic Water (pink) is revealed by our measurements in summer (4 August 2007; bold lines) and early winter (11 October 2006; thin lines). The main habitat of planktic foraminifers in the eastern Fram Strait (*16*, *18*) is marked by a dashed pattern.

Planktic foraminifer associations are useful indicators of water mass distributions and oceanic fronts in the northernmost North Atlantic (*17*). The planktic foraminiferal data from core MSM5/5-712-1 reveal multicentennial changes underlying a high-frequency (multidecadal) variability (Fig. 3A; for details of species distributions, see fig. S1). High flux rates of both polar and subpolar species characterize the RWP, the MCA-LIA transition, and the Modern Period, whereas low fluxes are recorded for the DACP and the late LIA (Fig. 3A). These flux variations likely reflect sea ice cover, because lowest planktic foraminiferal fluxes are today found in the ice-covered areas of the Fram Strait, and highest fluxes at the ice margins (*18*). In sediments from before ~1900 CE, 10 to 40% of all planktic foraminifers belong to subpolar species. In contrast, the youngest sediments reflecting the past ~100 years show a steep increase in subpolar foraminifer fluxes and an unprecedented inversion of the subpolar/polar species ratio, reaching 66% subpolar specimens in the surface sample (Fig. 3B). Because the percentage of subpolar specimens is closely related to the water mass distribution, with low values in Arctic waters and high values in AW (*16*–*18*), highest subpolar foraminifer fluxes and percentages in samples from the Modern Period indicate a strongly increased influence of warm AW advected from the Norwegian Sea.

Results from SIMMAX and Mg/Ca measurements allowed us to quantify the temperature increase associated with the stronger influence of AW off Western Svalbard during the Modern Period. Until ~1850 CE, average summer temperatures varied between 2.8° and 4.4°C (mean ± SE: 3.4° ± 0.06°C) according to SIMMAX, with low values during the well-known cold periods

(early DACP, LIA) and maxima during the early MCA at 800 to 1100 CE (Fig. 3C). The record shows strong similarities to terrestrial records of Northern Hemispheric and circum-Arctic temperature variability (*6*, *19*) (Fig. 3E). AW temperatures since 1890 CE were 4.1° to 6.0°C (mean ± SE: 5.2° ± 0.22°C) and thus ~2°C higher than during the previous 2 ky. The rapid increase to an unprecedented maximum of 6°C calculated for the surface sample apparently started already around 1850 CE. However, the gradual transition may be an artifact caused by bioturbation mixing of foraminifer-poor sediments from the late LIA and foraminifer-rich sediments from the Modern Period. Temperature reconstructions from Mg/Ca measurements give results very similar to those of SIMMAX (Fig. 3D). Variability before the Modern Period is high (0.7° to 5.7°C), probably because the Mg/Ca method could not precisely reproduce temperatures below 3°C [(*20*); see discussion in the SOM], but the temperature mean of 3.6°C (±0.3°C, SE) confirms the SIMMAX results. The same agreement applies for the Modern Period: Temperatures since 1890, as calculated from Mg/Ca data, range from 4.4 to 7.1 with a mean value of 5.8°C (±0.5°C, SE). For both methods, the temperature mean of the Modern Period exceeds all individual values from the preceding 2000 years. These results reveal a rapid warming by ~2°C of uppermost AW in the FSB in the Arctic Gateway during the past ~120 years, consistent with the documented sea ice retreat in the Barents Sea (*5*), terrestrial paleoclimate reference records (*6*, *19*) (Fig. 3, C to E), and atmospheric measurements (*3*). Notably, modern summer temperatures of uppermost AW in the eastern Fram Strait are >1.5°C higher than multidecadal mean temperature maxima (averaged by bioturbation and sampling) during the MCA.

Our reconstructed warming of ~2°C since the LIA matches the reported temperature increase of the Arctic Atlantic Water Layer (AAWL), obtained from observational data of the past ~120 years (*21*) (Fig. 3C). At present, there are no subcentennial-scale open ocean proxy data series available to document the temperature evolution of AAWL in the Arctic Ocean proper in the preceding two millennia. Further upstream, in the eastern Norwegian Sea, high-resolution records of summer sea surface temperature (SSST) variability from diatoms (*22*) and stable isotopes of planktic foraminifera (*23*) indicate a warming of ~1.5°C off western Norway since the LIA. However, eastern Norwegian Sea SSSTs in the late 1990s do not clearly deviate from those occurring periodically during the MCA (*22*, *23*). Our finding of unequaled warm modern AW temperatures in the eastern Fram Strait with respect to the previous 2000 years (including the warm periods in Roman and Medieval times) may thus express another facet of the Arctic amplification (*1*, *24*) of global warming. Recent model results (*25*, *26*) reveal the important role of sea ice and atmospheric pressure fields in the Barents Sea as

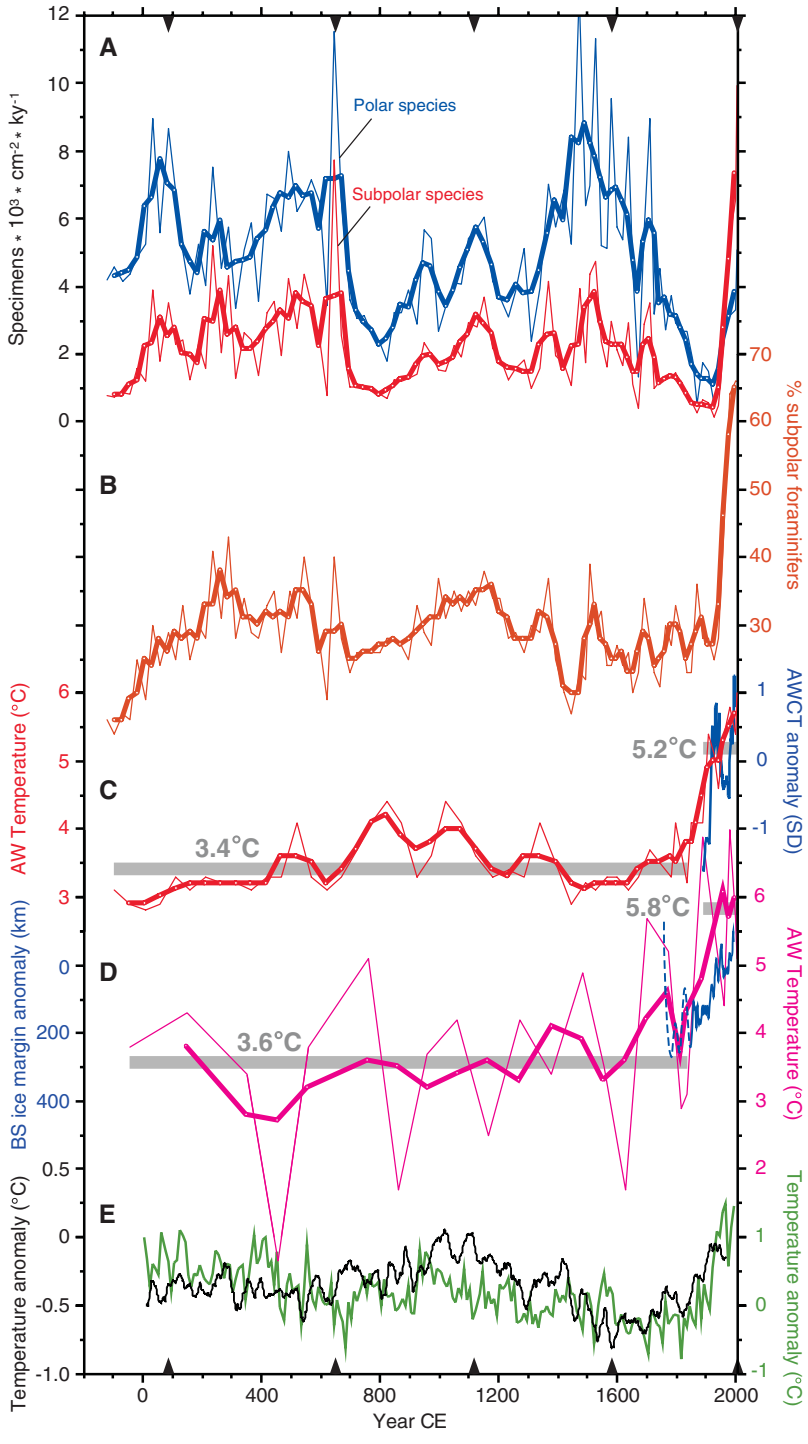

Fig. 3. Planktic foraminiferal data and temperature reconstructions of upper Atlantic Water in the eastern Fram Strait over the past ~2100 years from sediment core MSM5/5-712-1. Thin lines are raw data, bold lines are three-point running means. Black triangles on the age scale mark calibrated accelerator mass spectrometry ^{14}C ages. (**A**) Fluxes of polar and subpolar planktic foraminifers (100- to 250-μm fraction). (**B**) Percentage of subpolar planktic foraminifers in the 100- to 250-μm fraction. (**C**) Summer temperatures at 50-m water depth (red) calculated by the SIMMAX Modern Analog Technique. Gray bars mark averages until 1835 CE and 1890 to 2007 CE. Blue line is the normalized Atlantic Water core temperature (AWCT) record (standard deviations) from the Arctic Ocean (1895 to 2002; 6-year averages) obtained from (*21*). (**D**) Summer temperatures (purple) calculated from Mg/Ca ratios in planktic foraminifers *N. pachyderma* (sinistral). Gray bars mark averages until 1835 CE and 1890 to 2007 CE. Blue line is the sea ice margin anomaly (11-year means, less ice is up) in the Barents Sea (BS) obtained from (*5*). Dashed lines mark less reliable data before 1850 CE. (**E**) Terrestrial Arctic [green, from (*6*)] and Northern Hemisphere [black, 25-year means, from (*19*)] temperature anomaly records with reference to the 980 to 1800 CE and 1961 to 1990 CE averages, respectively.

a possible amplifier, which may, at least in part, be responsible for the exceptionally warm AW advection.

Instrumental air and AW temperatures in the Arctic during the 20th century and beyond display quasi-synchronous multidecadal oscillations that make isolation of the industrial warming trend difficult (*3*, *21*). Basinwide observations since the 1980s detected multiyear events of AW spreading in the Arctic Ocean that featured both a strong warming and an increased inflow to the Arctic (*7*, *27*, *28*). Although we cannot quantify from our data the variability of previous AW inflow to the Arctic by volume, our temperature data series and the above observational link suggest that the modern warm AW inflow (averaged over two to three decades) is anomalous and unique in the past 2000 years and not just the latest in a series of natural multidecadal oscillations. Both effects—a temperature rise as well as a volume transport increase—introduce a larger heat input into the Arctic Ocean. Although there is no direct contact of the AAWL with the ocean surface in the Arctic, such an increased heat input has far-reaching consequences. The strong AW warming event in the Arctic Ocean in the 1990s caused a shoaling of the AW core and an enhanced heat flux to the surface (*29*), concurrent with decreasing sea ice (*4*). Recent oceanographic data from the Laptev Sea continental margin indicate the impact of warm AW-related water masses on the shallow (<50 m) shelf (*30*), a feature not observed before in a >80-year time series. The data also provide evidence for a significant heat flux to the overlying shelf waters (*30*). Even without any modification of the vertical heat transfer processes, the enhanced temperature contrast between the AW and the surface sea water freezing point (increased from ~5 to 7 K as identified here) leads to an increase in the vertical heat flux of ~40%. Any positive-feedback mechanism will magnify the effect of this flux increase on the ice cover. Complementing the strong feedback between ice and atmospheric temperatures (*1*), warming of the AW layer, unprecedented in the past 2000 years, is most likely another key element in the transition toward a future ice-free Arctic Ocean.

References and Notes

1. J. A. Screen, I. Simmonds, *Nature* **464**, 1334 (2010).
2. R. G. Graversen, T. Mauritsen, M. Tjernström, E. Källén, G. Svensson, *Nature* **451**, 53 (2008).
3. P. Chylek, C. K. Folland, G. Lesins, M. K. Dubey, M. Muyin Wang, *Geophys. Res. Lett.* **36**, L14801 (2009).
4. J. C. Comiso, C. L. Parkinson, R. Gersten, L. Stock, *Geophys. Res. Lett.* **35**, L01703 (2008).
5. D. V. Divine, C. Dick, *J. Geophys. Res.* **111**, C01001 (2006).
6. D. S. Kaufman *et al.*, *Science* **325**, 1236 (2009).
7. B. Rudels, E. P. Jones, L. G. Anderson, G. Kattner, in *The Polar Oceans and Their Role in Shaping the Global Environment*, O. M. Johannessen, R. D. Muench, J. E. Overland, Eds. (American Geophysical Union, Washington, DC, 1994), pp. 33–46.
8. U. Schauer, E. Fahrbach, S. Osterhus, G. Rohardt, *J. Geophys. Res.* **109**, C06026 (2004).
9. S. Bonnet, A. de Vernal, C. Hillaire-Marcel, T. Radi, K. Husum, *Mar. Micropaleontol.* **74**, 59 (2010).
10. D. Hebbeln, T. Dokken, E. S. Andersen, M. Hald, A. Elverhøi, *Nature* **370**, 357 (1994).
11. T. M. Dokken, M. Hald, *Geology* **24**, 599 (1996).
12. R. F. Spielhagen *et al.*, *Quat. Sci. Rev.* **23**, 1455 (2004).
13. M. Hald *et al.*, *Quat. Sci. Rev.* **26**, 3423 (2007).
14. H. H. Lamb, *Climate: Present, Past and Future* (Methuen, London, 1977).
15. U. Pflaumann, J. Duprat, C. Pujol, L. D. Labeyrie, *Paleoceanography* **11**, 15 (1996).
16. R. Volkmann, *J. Foraminiferal Res.* **30**, 157 (2000).
17. T. Johannessen, E. Jansen, A. Flatøy, A. C. Ravelo, in *Carbon Cycling in the Glacial Ocean: Constraints on the Ocean's Role in Global Change*, R. Zahn, T. F. Pedersen, M. A. Kaminski, L. Labeyrie, Eds. (Springer-Verlag, Berlin, 1994), pp. 61–85.
18. J. Carstens, D. Hebbeln, G. Wefer, *Mar. Micropaleontol.* **29**, 257 (1997).
19. A. Moberg, D. M. Sonechkin, K. Holmgren, N. M. Datsenko, W. Karlén, *Nature* **433**, 613 (2005).
20. R. Kozdon, A. Eisenhauer, M. Weinelt, M. Y. Meland, D. Nürnberg, *Geochem. Geophys. Geosyst.* **10**, Q03005 (2009).
21. I. V. Polyakov *et al.*, *J. Clim.* **17**, 4485 (2004).
22. N. Koç, E. Jansen, in *Climate Development and History of the North Atlantic Realm*, G. Wefer, W. H. Berger, K.-E. Behre, E. Jansen, Eds. (Springer-Verlag, Berlin, 2002), pp. 165–173.
23. D. Klitgaard Kristensen, H. P. Sejrup, H. Haflidason, I. M. Berstad, G. Mikalsen, *Paleoceanography* **19**, PA2007 (2004).
24. M. Serreze, J. A. Francis, *Clim. Change* **76**, 241 (2006).
25. H. Goosse, M. M. Holland, *J. Clim.* **18**, 3552 (2005).
26. V. A. Semenov, W. Park, M. Latif, *Geophys. Res. Lett.* **36**, L14709 (2009).
27. M. J. Karcher, R. Gerdes, F. Kauker, C. Köberle, *J. Geophys. Res.* **108**, 3034 (2003).
28. I. A. Dmitrenko *et al.*, *J. Geophys. Res.* **113**, C05023 (2008).
29. M. Steele, T. Boyd, *J. Geophys. Res.* **103**, 10419 (1998).
30. I. A. Dmitrenko *et al.*, *J. Geophys. Res.* **115**, C08010 (2010).
31. R. R. Dickson *et al.*, *J. Clim.* **13**, 2671 (2000).

32. We thank the captains, crews, and shipboard scientific parties of research vessels *Jan Mayen* and *Maria S. Merian* for assistance during cruises JM06-WP and MSM5/5. R.F.S. and K.W. acknowledge support from the German Research Foundation (Deutsche Forschungsgemeinschaft Priority Core Program 1266 INTERDYNAMIK, project HOVAG); R.F.S. received support from the Academy of Sciences, Humanities, and Literature, Mainz; and S.A.S., K.Z., K.H., and M.H. acknowledge support from the Norwegian Research Council (projects SciencePub and WARMPAST). All data are available at www.pangaea.de (doi:10.1594/PANGAEA.755114).

Supporting Online Material

www.sciencemag.org/cgi/content/full/331/6016/450/DC1
Methods
Fig. S1
Table S1
References

6 September 2010; accepted 20 December 2010
10.1126/science.1197397

The Southern Route "Out of Africa": Evidence for an Early Expansion of Modern Humans into Arabia

Simon J. Armitage,[1] Sabah A. Jasim,[2] Anthony E. Marks,[3] Adrian G. Parker,[4] Vitaly I. Usik,[5] Hans-Peter Uerpmann[6]*

The timing of the dispersal of anatomically modern humans (AMH) out of Africa is a fundamental question in human evolutionary studies. Existing data suggest a rapid coastal exodus via the Indian Ocean rim around 60,000 years ago. We present evidence from Jebel Faya, United Arab Emirates, demonstrating human presence in eastern Arabia during the last interglacial. The tool kit found at Jebel Faya has affinities to the late Middle Stone Age in northeast Africa, indicating that technological innovation was not necessary to facilitate migration into Arabia. Instead, we propose that low eustatic sea level and increased rainfall during the transition between marine isotope stages 6 and 5 allowed humans to populate Arabia. This evidence implies that AMH may have been present in South Asia before the Toba eruption (*1*).

The deserts of the Arabian Peninsula have been thought to represent a major obstacle for human dispersal out of Africa. AMH were present in East Africa by about 200 thousand years ago (ka) (*2*). It is likely that the first migration of AMH out of Africa occurred immediately before or during the last interglacial [marine isotope stage (MIS) 5e] (*3*). During MIS 6, the Afro-Asiatic arid belt was hyperarid, restricting movements of human populations out of Africa. Finds from Qafzeh and Skhul in the Near East, dated between 119 ± 18 and 81 ± 13 thousand years ago (ka) (*4*, *5*), suggest that AMH first migrated along the "Nile Corridor" and into the Levant. A later pulse from <65 to 40 ka is thought to have led to further colonization into Europe

[1]Department of Geography, Royal Holloway, University of London, Egham, Surrey TW20 0EX, UK. [2]Directorate of Antiquities, Department of Culture and Information, Government of Sharjah, United Arab Emirates. [3]Department of Anthropology, Southern Methodist University, 3225 Daniel Avenue, Heroy Building 408, Dallas, TX 75275, USA. [4]Department of Anthropology and Geography, School of Social Sciences and Law, Oxford Brookes University, Headington, Oxford OX3 0BP, UK. [5]Archaeological Museum, Institute of Archaeology, National Academy of Sciences, B. Khmelnitsky Street, 15, 01030 Kiev, Ukraine. [6]Center for Scientific Archaeology, Eberhard-Karls-University Tübingen, Rümelinstraße 23, 72070 Tübingen, Germany.

*To whom correspondence should be addressed. E-mail: hans-peter.uerpmann@uni-tuebingen.de